J Solid State Electrochem (2003) 7: 468–476
DOI 10.1007/s10008-002-0348-6

ORIGINAL PAPER

V.V. Kharton · E.V. Tsipis · A.A. Yaremchenko
N.P. Vyshatko · A.L. Shaula · E.N. Naumovich
J.R. Frade

Oxygen ionic and electronic transport in $Gd_{2-x}Ca_xTi_2O_{7-\delta}$ pyrochlores

Received: 12 August 2002 / Accepted: 20 November 2002 / Published online: 5 February 2003

Abstract Oxygen ion transference numbers for $Gd_{2-x}Ca_xTi_2O_{7-\delta}$ ($x = 0.10$–0.14) pyrochlore ceramics were determined at 973–1223 K by the modified e.m.f. and faradaic efficiency techniques, taking into account electrode polarization, and from the results on oxygen permeation. The ion transference numbers vary in the range 0.95–0.98 in air, increasing when the temperature or oxygen partial pressure decreases. The activation energies for the ionic and p-type electronic transport in air are 74–77 and 87–91 kJ/mol, respectively. The p-type conductivity and oxygen permeability of $Gd_2Ti_2O_7$-based pyrochlores can be adequately described by relationships common for other solid electrolytes. At temperatures below 1273 K under a gradient of $10\%H_2 + 90\%N_2$/air, average ion transference numbers for doped gadolinium titanate are not less than 0.97. Thermal expansion coefficients for $Gd_{2-x}Ca_xTi_2O_{7-\delta}$ ceramics, calculated from dilatometric data in air, are in the range $(10.4–10.6)\times10^{-6}$ K^{-1} at 400–1300 K.

Keywords Fuel cell · Gadolinium titanate · Ionic conductivity · Pyrochlore · Transference number

Introduction

Solid oxide fuel cells (SOFCs) attract a great deal of interest due to their high energy-conversion efficiency, fuel flexibility including the prospects to directly operate on natural gas, and environmental safety [1, 2, 3, 4, 5]. However, practical applications of SOFCs as alternative electric power generation systems are still limited for economic reasons, particularly as a result of the high costs of component materials. The SOFC-based generators could be commercially viable if their production costs were approximately 0.7 US$ per 1 W [2, 3], but at present the figure is several times higher. Further progress in this field requires, hence, developments of new economically feasible materials, with special attention given to solid oxide electrolytes as key components of the electrochemical devices [4, 6]. Solid electrolytes should possess ion transference numbers close to unity over a wide range of oxygen partial pressures, high ionic conductivity to achieve minimum ohmic losses, chemical and dimensional stability, and compatibility with other cell components under the fuel cell operating conditions.

Among other promising electrolyte materials, such as doped CeO_2 and $LaGaO_3$ (e.g. [1, 3, 6] and references cited therein), rare-earth pyrochlore phases based on $Gd_2Ti_2O_7$ were reported to satisfy these requirements to a considerable extent [4, 5, 6, 7, 8, 9, 10, 11, 12, 13]. The structure of the $A_2B_2O_7$ pyrochlore (space group *Fd*3*m*) can be considered as an ordered defective derivative of fluorite, with one of eight oxygen sites per unit formula being vacant, which may be important for the ionic conduction [12, 13]. Moreover, in some cases this lattice represents a three-dimensional interconnected tunnel network [9]. As for other solid electrolytes, acceptor-type doping of $Gd_2Ti_2O_7$ leads to significant enhancement of the oxygen ionic transport; a maximum ionic conductivity of $(3.3–4.9)\times10^{-2}$ S/cm at 1273 K was found for $Gd_{2-x}Ca_xTi_2O_{7-\delta}$ with $x = 0.10$–0.30 [7, 8]. Substitution of gadolinium with calcium was reported to increase p-type electronic conduction and to decrease n-type contribution to the total conductivity [8]. The values of oxygen ion transference numbers (t_o) of $Gd_{1.9}Ca0.1Ti_2O_{7-\delta}$ in pure oxygen, which may be estimated from the $p(O_2)$ dependencies of the total conductivity [7], are quite high, 0.90–0.95 at 1073–1223 K.

V.V. Kharton (✉) · E.V. Tsipis · A.A. Yaremchenko
N.P. Vyshatko · A.L. Shaula · J.R. Frade
Department of Ceramics and Glass Engineering,
CICECO, University of Aveiro, 3810-193 Aveiro, Portugal
E-mail: kharton@cv.ua.pt
Tel.: +351-234-370263
Fax: +351-234-425300

V.V. Kharton · E.N. Naumovich
Institute of Physicochemical Problems, Belarus State University,
14 Leningradskaya Str., 220050 Minsk, Republic of Belarus

Later, however, significantly lower values of the ionic conductivity and ion transference numbers were reported [9]. For $Gd_2Ti_2O_7$ ceramics containing 5–10 mol% calcium, the transference numbers determined by the classical e.m.f. method under an oxygen chemical potential gradient of 2.1×10^4/10 Pa at 873–1023 K were found to be as low as 0.2 [9]. The corresponding estimates of ionic conductivity were surprisingly low, in the ranges of 3×10^{-6}–2×10^{-5} and 8×10^{-8}–9×10^{-7} S/cm for 5 mol% and 10 mol% Ca-doped $Gd_2Ti_2O_7$, respectively [9]. The compositions exhibiting maximum ionic conduction in the system $(Gd,Ca)_2Ti_2O_{7-\delta}$ are also different, namely 10 mol% Ca according to Kramer et al. [7, 8] but 5 mol% according to Heider et al. [9]. In addition, one should note significant contradictions in the literature data on activation energy (E_a) for the ionic transport. For undoped $Gd_2Ti_2O_7$, E_a values calculated from experimental results on the oxygen ionic conductivity are 0.93 eV [8] and 2.3 eV [9], while the atomic-scale computer simulations of oxygen migration give a value of 1.23 eV [12]. These differences might be partly explained by cation disordering in the pyrochlore lattice [12, 14].

The present work continues our research on ionic and electronic conduction in potential solid electrolyte materials [15, 16, 17, 18, 19, 20, 21, 22] and is focused on the transport properties of $Gd_{2-x}Ca_xTi_2O_{7-\delta}$ ($x=0.10$–0.14). This narrow composition range was selected to match the compositions with most promising properties and to reassess contradictory literature data on pyrochlore phases with a significant level of ionic conductivity [7, 8, 9]. Although the conductivity of $Gd_{2-x}Ca_xTi_2O_{7-\delta}$ is relatively low [7, 8, 9], these materials are still of interest for electrochemical cells with film electrolytes, especially for monolithic SOFCs. In the latter case, pyrochlore phases may even be advantageous with respect to other solid electrolytes owing to a higher solid solubility of variable-valence dopants in the lattice, which makes it possible to form mixed-conducting electrodes with the same structure (e.g. [7, 8] and references therein). As oxygen diffusion in pyrochlores considerably depends on a partial cation disorder [12, 13, 14], special emphasis in this paper is given to the structural characterization of $Gd_{2-x}Ca_xTi_2O_{7-\delta}$ ceramics. Also, thermal expansion coefficients, which determine the compatibility with other materials of an electrochemical device, and the behavior of gadolinium titanate membranes in SOFC-type measuring cells were also studied.

Experimental

Single-phase powders of $Gd_{2-x}Ca_xTi_2O_{7-\delta}$ ($x=0.10$–0.14) were synthesized by a standard ceramic technique. Before weighing the stoichiometric amounts of high-purity $CaCO_3$, Gd_2O3 and TiO_2, the gadolinium and titanium oxides were annealed in air at 1173–1273 K for 2–3 h. The solid-state reactions were performed at 1273–1623 K for 35 h in air, with multiple intermediate regrindings. After confirming the formation of single pyrochlore phases by X-ray diffraction (XRD), the powders were compacted into disks of various thickness (diameter 20 mm, 250–300 MPa). Gas-tight ceramics were sintered in air during 4 h at 1823 K with subsequent slow cooling (3–5 K/min) down to room temperature, in order to obtain equilibrium oxygen nonstoichiometry. The density of the ceramic materials was higher than 98.5% of their theoretical density calculated from XRD data (Table 1).

XRD spectra of powders, obtained by grinding the ceramic samples, were collected at room temperature in the range of 2θ angles from 10° to 100° (step 0.02°, 2 s/step, Cu K_α radiation). Structure parameters were refined using the Fullprof program [23]. Transmission electron microscopy (TEM) studies of the powders were performed using a Hitachi H-9000 electron microscope with a beam voltage of 300 kV. Dilatometric data were obtained in air using a Linseis L70/2001 apparatus (heating rate of 3 K/min). The microstructure of the ceramics was studied by scanning electron microscopy combined with energy dispersive spectroscopy (SEM/EDS); AC impedance spectroscopy was used for the measurements of the total conductivity. Description of the experimental techniques and equipment can be found elsewhere ([15, 16, 17, 18, 19, 20, 21, 22] and references therein).

The oxygen ion transference numbers were determined by modified faradaic efficiency (FE) and e.m.f. (EMF) methods [21, 22], and also calculated from the oxygen permeability (OP) and total conductivity. It is well known [21, 22, 24] that decreasing temperature and/or oxygen partial pressure in the measuring cells leads to increasing errors in the transference number determination by the classical e.m.f. and faradaic efficiency techniques, owing to a greater role of electrode polarization; the apparent ion transference numbers become lower than the true t_o values. Therefore, in the present work the modifications of faradaic efficiency and e.m.f. methods, described elsewhere [21, 22], were used. These modifications make it possible to take electrode polarization into account and to increase accuracy of the transference number determination [21]; experimental details are available [19, 20, 21]. All measurements by the e.m.f. technique were performed under an oxygen partial pressure gradient at the electrodes (p_2/p_1) equal to 101/21 kPa. The faradaic efficiency measurements were performed under zero oxygen chemical potential gradient in air ($p_2=p_1=21$ kPa), and also at p_1 values that varied from 2 to 11 kPa at a fixed p_2 of 21 kPa. In the latter case, the results were

Table 1 Properties of $Gd_{2-x}Ca_xTi_2O_{7-\delta}$ ceramics

Composition (x)	d_{exp} (g/cm^3)[a]	d_{exp}/d_{theor} (%)[a]	$\bar{\alpha}\times10^6$ (K^{-1}) (400–1300 K)[b]	Activation energy for the total conductivity[c]		
				T (K)	E_a (kJ/mol)	ln A_0 (S K/cm)
0.10	6.19	98.9	10.54 ± 0.02	670–820	96 ± 5	14.1 ± 0.8
				820–1250	75 ± 2	10.9 ± 0.3
0.14	6.07	98.8	10.44 ± 0.03	500–820	97 ± 6	14.3 ± 0.9
				820–1270	74 ± 1	10.9 ± 0.1

[a]dexp and d_{theor} are the experimental and theoretical density values, respectively
[b]$\bar{\alpha}$ is the linear thermal expansion coefficient (TEC) in air, averaged over the temperature range 400–1300 K
[c]Ea and A_0 are the regression parameters of the Arrhenius model for total conductivity

corrected for the steady oxygen permeation fluxes, a priori independently measured. Testing of model fuel cells with pyrochlore ceramic membranes (thickness 1.00 mm, electrode area 0.6–0.7 cm^2) and porous Pt electrodes was carried out at 1123–1273 K using a flowing 10% H_2/90% N_2 mixture as fuel and air as oxidant (flow rate 250 mL/min). The current density varied from 0 to 80 mA/cm^2; ohmic contribution to the cell resistance was determined by impedance spectroscopy. The transference numbers of pyrochlore membranes in such cells were determined from the starting segments of the voltage versus load resistance curves at current density values lower than 10–15 mA/cm^2, with correction for the electrode polarization resistance [21, 22]. Experimental procedures for the oxygen permeation measurements are also reported elsewhere [25, 26].

Results and discussion

Characterization of ceramic materials

XRD studies of $Gd_{2-x}Ca_xTi_2O_{7-\delta}$ powders and ceramics showed the formation of single phases with a pyrochlore structure. An example of a final Rietveld plot, showing the quality of structure refinement, is given in Fig. 1. The unit cell parameters of the materials with $x = 0.10$ and 0.14 are quite similar, as the difference in their composition is rather small (Table 2). At the same time, the analysis of cation-anion bond lengths in the pyrochlore lattice indicates that Ti-O octahedra contract and their distortion decreases when the calcium concentration increases. These octahedra are formed by so-called O1 oxygen sites (position 48f mm u 1/8 1/8) and have an ideal form if $u = 0.3125$. Increasing x results in a clear decrease in the Ti-O1 distance, considerably larger than the experimental error; the parameter u for $Gd_{2-x}Ca_xTi_2O_{7-\delta}$ is higher than 0.3125, but decreases with x (Table 2).

As the pyrochlore structure is a cation-ordered derivative of the fluorite structure, a number of pyrochlore phases exhibit partial or complete disordering on heating; the latter process corresponds to a transformation of an $A_2B_2O_7$ pyrochlore into a nonstoichiometric $(A,B)O_{3.5\pm\delta}$ fluorite lattice, one example of which refers to 50 mol% yttria-doped zirconia [13, 27]. The lattice disorder leads, as a rule, to greater oxygen ionic conduction [13, 27]. Since partial cation disordering may also be induced by A-site doping [13], TEM examination of a $Gd_{1.9}Ca0_{.1}Ti_2O_{7-\delta}$ fine-ground ceramic sample was carried out. An example of the electron diffraction pattern is presented in Fig. 2. The inspection of the TEM results showed no evidence of cation disorder; the lattice parameters calculated from the XRD and TEM data were very similar, within the limits of experimental error. Taking into account that thermally induced cation disordering of pyrochlore-type compounds usually becomes significant only when the temperature is higher than 1350–1500 K [13, 27, 28], the level of structural disorder in $Gd_{2-x}Ca_xTi_2O_{7-\delta}$ is expected to be rather negligible and essentially unaffected by temperature variations within the studied range (400–1223 K).

Figure 3 presents SEM micrographs, reflecting microstructures characteristic of $Gd_{2-x}Ca_xTi_2O_{7-\delta}$ ceramics. The average grain size is similar for both studied

Table 2 Structure refinement results for $Gd_{2-x}Ca_xTi_2O_{7-\delta}$

	$Gd_{1.90}Ca_{0.10}Ti_2O_{7-\delta}$	$Gd_{1.86}Ca_{0.14}Ti_2O_{7-\delta}$
Crystal system	Cubic	
Spacegroup	*Fd3m* (no 227)	
Unit cell parameter (Å)	10.192(5)	10.193(1)
u	0.32431	0.32258
Interatomic distances (Å)		
Ti-O1	1.955	1.948
Ti-O2	2.226	2.226
Gd-O1	2.540	2.553
Gd-O2	2.207	2.207
O1-O1	2.651	2.658
O1-O2	3.065	3.083
O2-O2	4.413	4.414

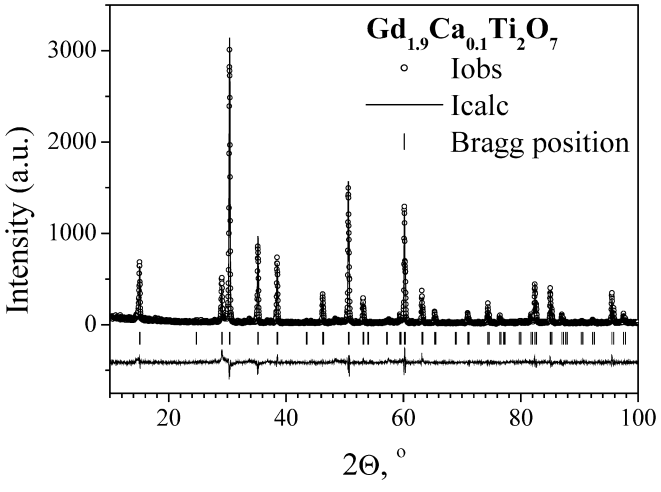

Fig. 1 Observed, calculated and difference XRD patterns of $Gd_{1.90}Ca0_{.10}Ti_2O_{7-\delta}$

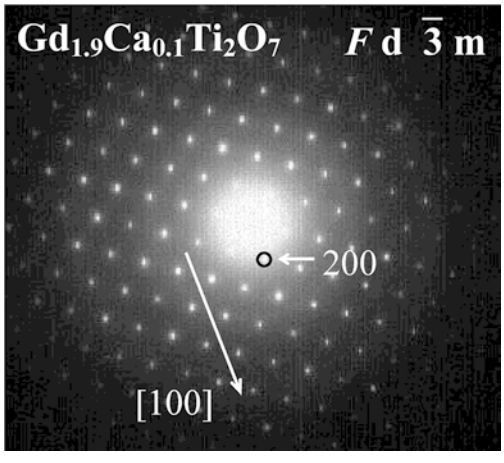

Fig. 2 Transmission electron diffraction pattern of $Gd_{1.90}Ca_{0.10}Ti_2O_{7-\delta}$

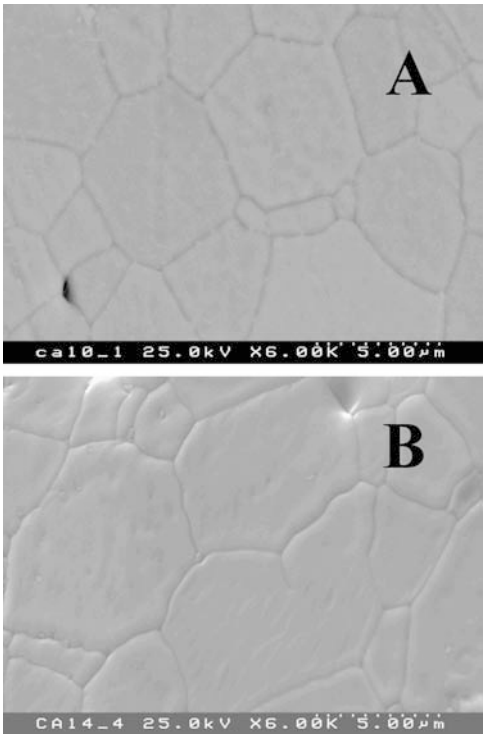

Fig. 3 SEM micrographs of $Gd_{2-x}Ca_xTi_2O_{7-\delta}$ ceramics with $x = 0.10$ (**A**) and 0.14 (**B**)

compositions and varies in the range 5–10 μm. In agreement with the picnometric data (Table 1), the closed porosity of the ceramic materials was very small. No traces of liquid phase formation at the grain boundaries or phase impurities were detected by SEM/EDS analysis.

Dilatometric curves of $Gd_{2-x}Ca_xTi_2O_{7-\delta}$ ceramics are close to linear within all studied temperature ranges, 400–1300 K (Fig. 4). The average thermal expansion coefficients (TECs) calculated from dilatometric data vary in the very narrow range $(10.4–10.6)\times10^{-6}$ K^{-1} (Table 2). These TEC values are very similar to literature data on $Y_2(Ti,Zr)_2O_7$ pyrochlores [13] and to the TECs of stabilized zirconia ceramics [27].

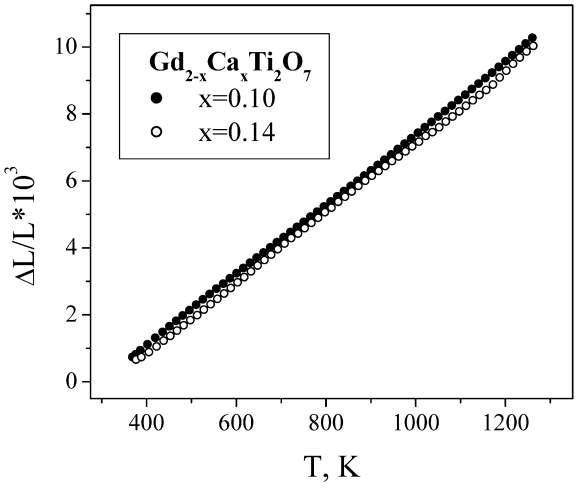

Fig. 4 Dilatometric curves of $Gd_{2-x}Ca_xTi_2O_{7-\delta}$ ceramics in air

Total conductivity

The temperature dependence of the total conductivity (σ) of $Gd_{2-x}Ca_xTi_2O_{7-\delta}$ is shown in Fig. 5. The conductivity is predominantly oxygen ionic (Table 3) and excellently coincides with the results of Kramer and Tuller [7]. The significantly lower conduction level of the same compositions [9] may therefore result from specific features of $Gd_{2-x}Ca_xTi_2O_{7-\delta}$ ceramics sintered at 1373 K, such as blocking grain boundaries in ceramics with fine grain sizes. Indeed, in the case of zirconia-based materials, low sintering temperatures are typically associated with a greater grain-boundary resistance [27].

The conductivity of $Gd_{1.86}Ca_{0.14}Ti_2O_{7-\delta}$ at temperatures above 823 K is slightly higher than that of $Gd_{1.90}Ca_{0.10}Ti_2O_{7-\delta}$, whereas in the low-temperature range the σ values of both compositions are similar. The activation energy for the total conductivity, calculated by the standard Arrhenius equation:

$$\sigma = \frac{A_0}{T}\exp\left[-\frac{E_a}{RT}\right] \quad (1)$$

where A_0 is the pre-exponential factor, increases from 74–75 kJ/mol at 823–1273 K up to 96–97 kJ/mol at 500–823 K (Table 1). According to the TEM results and literature data [13, 27, 28], cation disordering of the pyrochlore titanates at temperatures around 800–850 K seems unlikely. The impedance spectroscopic data, examples of which are presented below, indicate a negligible contribution of the grain boundaries to the total resistance within all studied temperature ranges (400–1300 K); the change in the activation energy at 823 K cannot thus be attributed to grain-boundary effects.

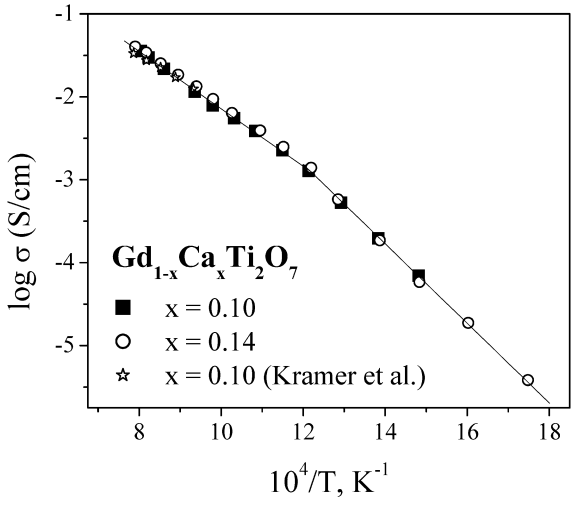

Fig. 5 Temperature dependence of the total conductivity of $Gd_{2-x}Ca_xTi_2O_{7-\delta}$ ceramics in air. Data on $Gd_{1.90}Ca_{0.10}Ti_2O_{7-\delta}$ [5] are shown for comparison

Table 3 Parameters for oxygen ionic transport in $Gd_{2-x}Ca_xTi_2O_{7-\delta}$ ceramics in air

Composition (x)	Averageion transference numbers[a]			Activationenergy for ionic and electron-hole conductivities (973–1223 K)[b]	
	T (K)	$\bar{t}_o$ (EMF)	$\bar{t}_o$ (FE)	$E_a(\sigma_o)$ (kJ/mol)	$E_a(\sigma_p)$ (kJ/mol)
0.10	1223	0.952	0.952	77 ± 4	91 ± 2
	1173	0.956	0.955		
	1123	0.958	0.958		
	1073	0.960	0.959		
	1023	0.961	0.962		
	973	–	0.967		
0.14	1223	0.960	0.956	74 ± 2	87 ± 3
	1173	0.966	0.958		
	1123	0.968	0.960		
	1073	0.972	0.962		
	1023	–	0.965		
	973	–	0.968		

[a]Each t_o value was averaged from 2–4 experimental data points

[b]The oxygen ionic conductivity was calculated from the results on the total conductivity and transference numbers, determined by the faradaic efficiency method, as $\sigma_o = \sigma t_o$

Most probably, the observed change in E_a values is due to disordering in the oxygen sublattice on heating, which is quite typical for stabilized zirconia and hafnia [27, 28]. The composition-independent conductivity in the low-temperature range may result from an association of oxygen vacancies and calcium cations and/or from formation of ordered microdomains. At temperatures above 823 K, disordering in the oxygen sublattice leads to a lower activation energy due to decreasing contribution of the vacancy formation energy to E_a values down to zero; ionic conduction in the high-temperature range becomes dependent on the total oxygen-vacancy concentration, which increases with calcium content (Fig. 5).

The impedance spectroscopic studies of $Gd_{2-x}Ca_xTi_2O_{7-\delta}$ ceramics demonstrated that in the studied temperature range the grain-boundary resistance can be neglected. At all temperatures, only two arcs were observed in the impedance spectra; the high-frequency arc with a specific capacitance of about 10^{-12} F/cm is obviously associated with grain bulk conduction, whilst the low-frequency part of the spectra (10^{-7}–10^{-6} F/cm) corresponds to electrode processes. Representative examples of the impedance spectra at different temperatures are given in Fig. 6A and Fig. 6B. For comparison, Fig. 6C presents the data for $Gd_{2-x}Ca_xTi_2O_{7-\delta}$ ceramics containing approximately 1.5 mol% of SiO_2. Silica impurities are well known to segregate at grain boundaries of most solid-electrolyte ceramics and to dramatically increase boundary resistivity [27, 29, 30]. As for other solid electrolytes, additions of SiO_2 lead to the appearance of a new intermediate-frequency arc in the impedance spectra of pyrochlore titanates (Fig. 6C). This arc, having a specific capacity of (4–9)×10^{-9} F/cm at 773 K, can be undoubtedly attributed to the grain-boundary processes. The example shown in Fig. 6C stresses that the measurement conditions used in this work provided sufficient sensitivity for the grain-boundary effects; the absence of intermediate-frequency phenomena in the impedance spectra of pure $Gd_{2-x}Ca_xTi_2O_{7-\delta}$ ceramics is conclusive proof of the negligible boundary contribution to the total resistance.

Transference numbers in oxidizing conditions

The oxygen ion transference numbers for $Gd_{2-x}Ca_xTi_2O_{7-\delta}$ at 973–1223 K, determined by the modified faradaic efficiency technique under zero oxygen chemical potential gradient in air, vary from 0.95 to 0.97, slightly increasing when the temperature decreases or the calcium concentration increases (Table 3). The e.m.f. method under an oxygen/air gradient gives very similar values for the transference numbers (Table 3) and for the electronic conductivity (Fig. 7). This confirms the correctness of the measurement techniques and the reliability of the results.

Tuller et al. [6, 7, 8] showed that the electronic conductivity of $Gd_{2-x}Ca_xTi_2O_{7-\delta}$ in oxidizing conditions is predominantly p-type; the n-type contribution is negligibly small. Therefore, the equilibrium ion transference numbers can be written as [31]:

$$t_o = \frac{\sigma_o}{\sigma_o + \sigma_p} = \frac{\sigma_o}{\sigma_o + \sigma_{p0} \times p(O_2)^{1/m}} \quad (2)$$

where σ_o and σ_p are the partial ionic and p-type electronic conductivities, respectively, σ_{p0} is the electron-hole conductivity at unit oxygen pressure, and m is a constant typically close to 4 for solid electrolytes. According to Tuller and Kramer [6, 7], ionic conduction in $(Gd,Ca)_2Ti_2O_{7-\delta}$ phases is independent of the oxygen partial pressure, which also agrees with the data on many other solid electrolytes [27, 28, 31]. For the measurements under a non-zero oxygen pressure gradient, either by e.m.f. or the faradaic efficiency technique, the transference numbers are averaged in a given range of oxygen chemical potentials (μ):

$$\bar{t}_o = \frac{1}{\mu_2 - \mu_1} \int_{\mu_1}^{\mu_2} t_o \, d\mu \quad (3)$$

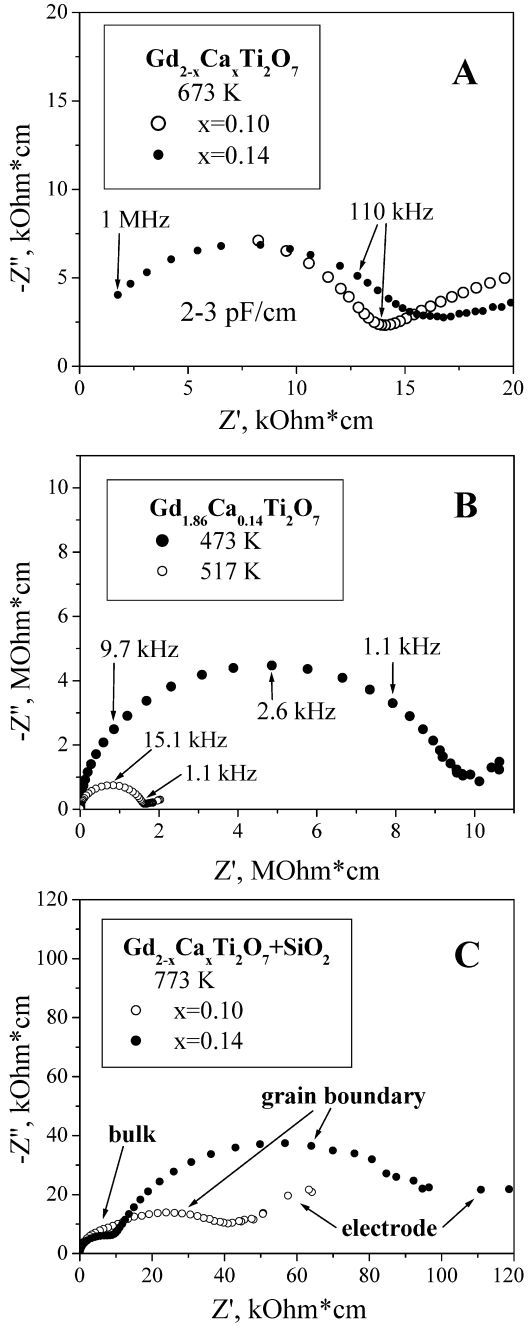

Fig. 6 Typical impedance spectra of $Gd_{2-x}Ca_xTi_2O_{7-\delta}$ samples in air: **A**, **B** pure ceramic materials studied in this work; **C** ceramics with SiO_2 additions

where the values of μ_1 and μ_2 correspond to $p(O_2)$ values at the electrodes, p_1 and p_2. Substitution of Eq. 2 into Eq. 3 and integration results in the following expression:

$$\bar{t}_o(p_2, p_1) = -m \ln \frac{k_1 p_2^{-1/m} + 1}{k_1 p_1^{-1/m} + 1} \left(\ln \frac{p_2}{p_1} \right)^{-1} \quad (4)$$

where $k_1 = \sigma_o/\sigma_{p0}$. Figure 8A shows the fitting of the results of the experimental dependence of the average transference numbers on p_1, determined by faradaic efficiency measurements at a fixed $p_2 = 21$ kPa, using Eq. 4

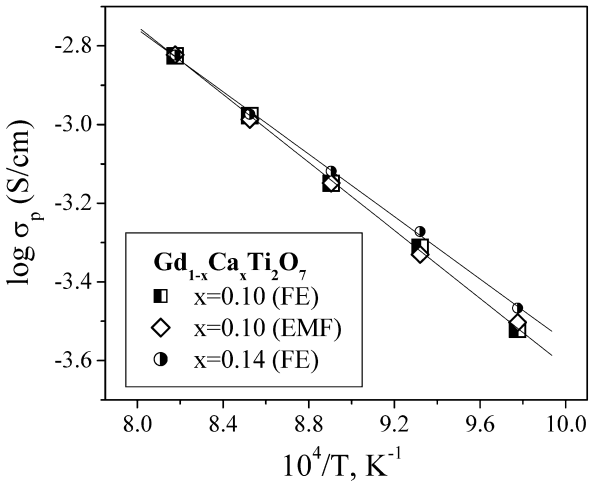

Fig. 7 Temperature dependence of the p-type electronic conductivity of $Gd_{2-x}Ca_xTi_2O_{7-\delta}$ ceramics in air, calculated from the impedance spectroscopy, faradaic efficiency and e.m.f. results

as a regression model. Taking into account experimental error, this equation is considered to be adequate. The calculated value of the m parameter, 4.7 ± 0.2, is quite close to 4, the classical value for electron-hole transport in solid electrolytes.

Under these conditions, if the surface exchange limitations to the overall oxygen transport through a pyrochlore membrane can be neglected, the permeation flux density (j) is described as:

$$j = \frac{1}{16F^2 d} \int_{\mu_1}^{\mu_2} \frac{\sigma_o \sigma_p}{\sigma_o + \sigma_p} d\mu = \frac{1}{16F^2 d} \int_{\mu_1}^{\mu_2} t_o(1 - t_o)\sigma \, d\mu \quad (5)$$

where d is the membrane thickness. After substitution of Eq. 2, the analytical solution of Eq. 5 is:

$$j = \frac{RTm\sigma_o}{16F^2 d} \ln \frac{\sigma_{p0} p_2^{1/m} + \sigma_o}{\sigma_{p0} p_1^{1/m} + \sigma_o} \quad (6)$$

Figure 8B compares the experimental results on oxygen permeation through a $Gd_{1.90}Ca_{0.10}Ti_2O_{7-\delta}$ membrane and the corresponding predictions, calculated by Eq. 6, with the values of m, σ_o and σ_{p0} obtained by other methods. The parameters m and k_1 were determined by fitting of $\bar{t}_o$ versus p_1 dependence obtained by FE measurements (Fig. 8A); the values of σ_o and σ_{p0} were extracted from the total conductivity in air (Fig. 5) using the definitions $k_1 = \sigma_o/\sigma_{p0}$ and $\sigma = \sigma_o + \sigma_{p0} \times p(O_2)^{1/m}$. The experimentally measured and calculated permeation fluxes are very similar (Fig. 8B), thus confirming that the different methods are consistent with each other and that Eq. 6 is valid.

Figure 8C presents the equilibrium transference numbers, t_o, which were evaluated from the regression parameters of $\bar{t}_o - p_1$ and $j - p_1$ dependencies (Fig. 8A, B) expressed by Eqs. 4 and 6, respectively. Again, the results obtained using different measurement techniques are similar within the limits of experimental uncertainty. Thus, p-type electronic conductivity and oxygen

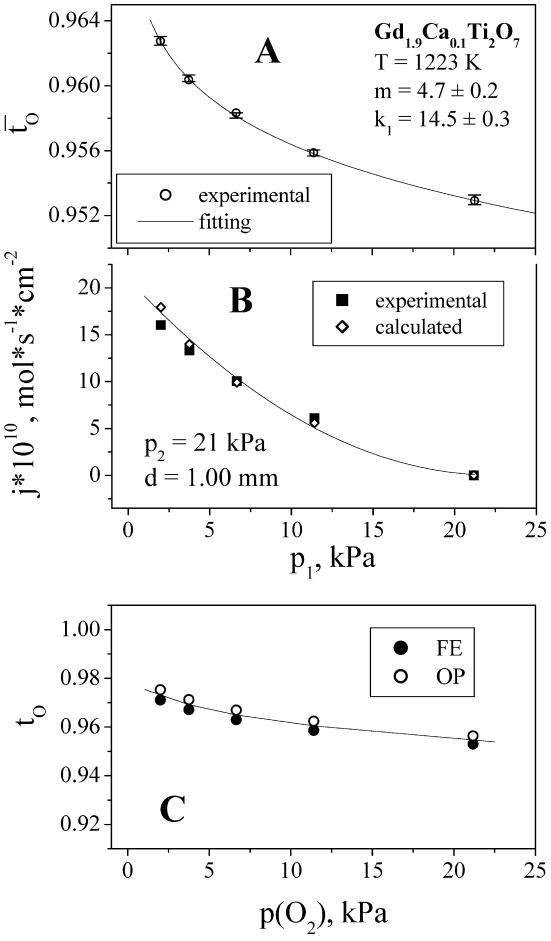

Fig. 8 Dependencies of the average ion transference numbers (**A**) and oxygen permeation flux density (**B**) on the permeate-side oxygen pressure, and $p(O_2)$ dependence of equilibrium transference numbers of $Gd_{1.90}Ca_{0.10}Ti_2O_{7-\delta}$ at 1223 K calculated from these results (**C**). *Solid line* in **A** corresponds to best fit to the faradaic efficiency data using Eq. 4 as a regression model. *Solid lines* in **B** and **C** are for visual guidance only

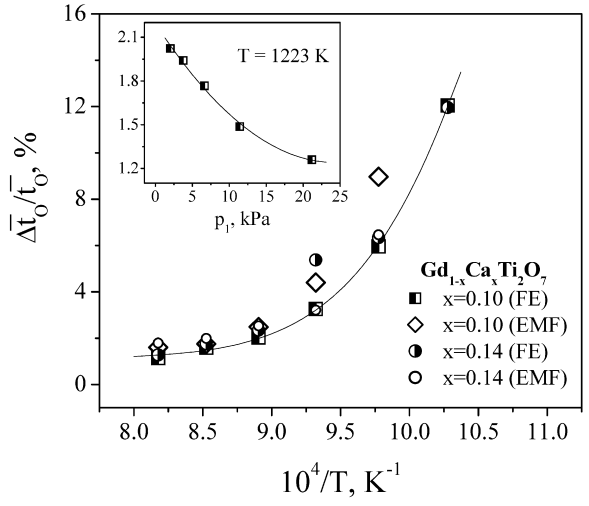

Fig. 9 Relative error of the transference number determination by classical e.m.f. and faradaic efficiency methods, appearing due to electrode polarization. *Inset* shows the same quantity as a function of p_1 at 1223 K

permeability of $Gd_{2-x}Ca_xTi_2O_{7-\delta}$ pyrochlores can both be adequately described by models, derived from relationships common for other solid electrolytes [27, 31].

Finally, Fig. 9 shows the relative error in the ion transference numbers ($\bar{t}_o^{obs}$) determined by classical e.m.f. and faradaic efficiency methods, which appears due to electrode polarization in the measuring cells. The error was evaluated as:

$$(\Delta\bar{t}_o/\bar{t}_o) = (\bar{t}_o - \bar{t}_o^{obs})/\bar{t}_o \quad (7)$$

where $\bar{t}_o$ values were measured by the modified techniques, taking polarization resistance into account. For the classical e.m.f. method [31], the transference numbers are estimated as the ratio between the observed e.m.f. of an oxygen concentration cell and its theoretical Nernst voltage; in the case of the classical arrangement of the faradaic efficiency measurements, ionic contribution to the total conductivity is estimated from the ratio of the ionic and total currents through a mixed conductor. However, when electrode polarization is significant, these apparent transference numbers are considerably lower than the true t_o values. The relative error increases with decreasing oxygen partial pressure and temperature (Fig. 9). A detailed analysis of this issue can be found elsewhere [21, 22]; in this work, one can briefly note that the behavior of $(Gd,Ca)_2Ti_2O_{7-\delta}$, illustrated by Fig. 9, is similar to other solid electrolytes, such as doped γ-$Bi_2VO_{5.5-\delta}$ [19], $LaGaO_3$ [20], $CeO_{2-\delta}$ [21] and $BaCeO_{3-\delta}$ [24]. Most probably, this error may constitute a reason for the very low apparent transference numbers reported by Heider et al. [9].

Partial ionic and p-type electronic conductivities

Increasing the calcium content in the $Gd_{2-x}Ca_xTi_2O_{7-\delta}$ lattice leads to a slight decrease in the activation energy for electron-hole transport in air (Table 3). As a result, the p-type conductivity of $Gd_{1.90}Ca_{0.10}Ti_2O_{7-\delta}$ at temperatures below 1100 K is lower than that of $Gd_{1.86}Ca_{0.14}Ti_2O_{7-\delta}$; at higher temperatures the σ_p values are essentially independent of x (Fig. 7). This phenomenon indicates that charge compensation of acceptor-type doping occurs via oxygen vacancy formation rather than via generation of any positive electronic charge carriers, which seems quite reasonable as the oxidation state of the cations in the structure of $Gd_{2-x}Ca_xTi_2O_{7-\delta}$ cannot increase further . The electron-hole conduction is therefore related to intrinsic electronic disorder, at least in the high-temperature range.

Owing to the charge compensation mechanism via oxygen vacancy formation, doping with calcium leads to increasing oxygen ionic conductivity (Fig. 10). The observed activation energy for ionic transport, 74–77 kJ/mol at 973–1223 K (Table 3), is slightly higher compared to the data by Kramer and Tuller [7], who reported E_a values for $Gd_{2-x}Ca_xTi_2O_{7-\delta}$ ($x = 0.10$–0.20) in the range 63–65 kJ/mol at 1073–1373 K. Such a

difference may result from the different temperature ranges studied in the present work and by Kramer and Tuller [7]. For instance, the activation energy for ionic conduction in stabilized zirconia typically increases with decreasing temperature, owing to a progressive association of mobile oxygen vacancies [27]. The values of E_a, calculated for $Gd_{2-x}Ca_xTi_2O_{7-\delta}$ ceramics, are comparable with those of well-known solid electrolytes, such as gadolinia-doped ceria (CGO) or $La(Sr)Ga(Mg)O_{3-\delta}$ (LSGM) [17, 29, 32]. However, the level of ionic conductivity in $(Gd,Ca)_2Ti_2O_{7-\delta}$ is lower by 8–10 times (Fig. 10).

Transport properties under fuel cell operation conditions

The measurements of oxygen ion transference numbers by the modified e.m.f. method, performed under the gradient of $10\%H_2 + 90\%N_2$/air, showed that in fuel cell operating conditions the electronic contribution to the total conductivity of $Gd_{2-x}Ca_xTi_2O_{7-\delta}$ is relatively small, less than 3% (Table 4). This behavior is similar to LSGM electrolytes; the n-type electronic conduction induced in CGO ceramics in H_2-containing atmospheres is considerably higher (see [17] and references therein). Hence, a decrease in the performance of SOFCs with pyrochlore solid electrolytes owing to their electronic conductivity is expected to be rather negligible.

However, owing to the low ionic conductivity of $(Gd,Ca)_2Ti_2O_{7-\delta}$ ceramics (Fig. 10), the ohmic losses in model fuel cells with pyrochlore electrolytes are excessively high, resulting in a poor cell performance even at temperatures as high as 1223–1273 K (Fig. 11). Figure 11A shows one example of the ohmic losses (*IR*) in a cell with a $Gd_{1.90}Ca_{0.10}Ti_2O_{7-\delta}$ electrolyte membrane, calculated from the impedance spectroscopy data and marked by open squares. The ohmic contribution to the total voltage drop is up to 70%. This leads to almost linear current-voltage curves.

The maximum power density, shown by the cells with a $(Gd,Ca)_2Ti_2O_{7-\delta}$ electrolyte and porous Pt electrodes, at 1123–1273 K varied from 8 to 18 mW/cm^2, increasing with temperature (Fig. 11). Such a performance is 10–20 times lower than the minimum necessary for commercial use. At the same time, a definite improvement can be achieved by enhancing the electrochemical activity of the electrodes and by decreasing the electrolyte thickness. Therefore, owing to low ionic conductivity of $(Gd,Ca)_2Ti_2O_{7-\delta}$, possible applications of these materials may be in electrode-supported fuel cells where the thickness of the solid-electrolyte film is less than 50–100 μm. The sufficiently high stability of the pyrochlore

Table 4 Average ion transference numbers for $Gd_{1.90}Ca0_{.10}Ti_2O_{7-\delta}$ under a $10\%H_2 + 90\%N_2$/air gradient, determined by the modified e.m.f. method

T (K)	$\bar{t}_o$
1273	0.976 ± 0.001
1223	0.982 ± 0.001
1123	0.989 ± 0.002

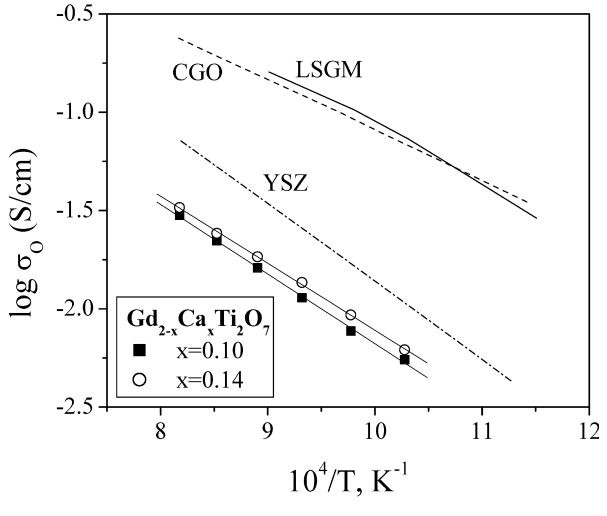

Fig. 10 Temperature dependence of the oxygen ionic conductivity of $Gd_{2-x}Ca_xTi_2O_{7-\delta}$ in air. Data on $La_{0.80}Sr_{0.20}Ga_{0.85}Mg_{0.15}O_{3-\delta}$ (LSGM), $Ce_{0.80}Gd_{0.20}O_{2-\delta}$ (CGO) and $Zr_{0.90}Y_{0.10}O_{1.95}$ (YSZ) [32] are shown for comparison

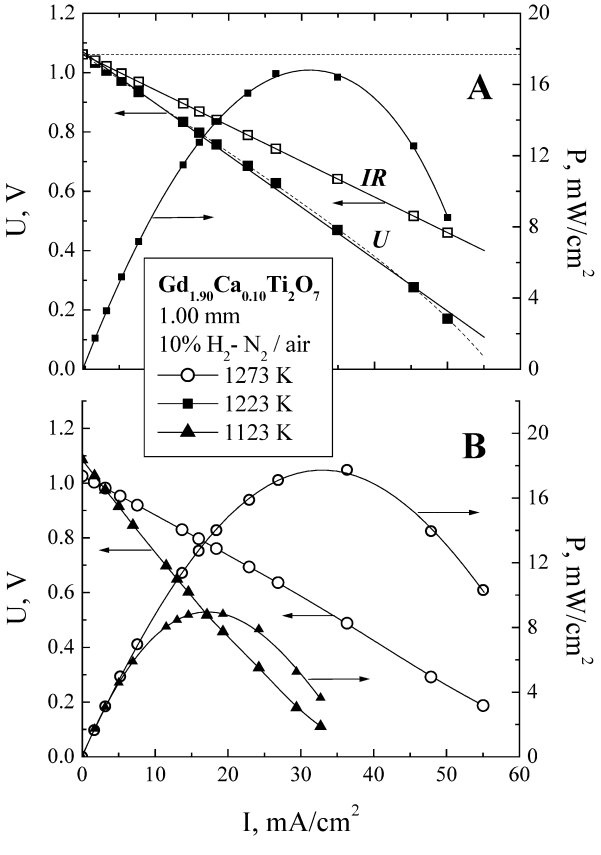

Fig. 11 Current dependencies of the voltage and specific power density of a model fuel cell: $10\%H_2 + N_2$,Pt|$Gd_{1.9}Ca_{0.1}Ti_2O_7$|Pt,O_2(air). *Solid* and *open squares* in **A** show the voltage (U) and ohmic losses (*IR*), respectively

phases in reducing environments and the moderate thermal expansion might be advantageous for these applications.

Conclusions

Single-phase $Gd_{2-x}Ca_xTi_2O_{7-\delta}$ ($x = 0.10$–0.14) ceramics with a density higher than 98% of the theoretical density were prepared by the standard solid-state synthesis route. The average thermal expansion coefficients (TECs) in air are in the range $(10.4–10.6)\times10^{-6}$ K^{-1} at 400–1300 K. No indication of partial cation disorder was found by TEM. Oxygen ion transference numbers for $Gd_{2-x}Ca_xTi_2O_{7-\delta}$ pyrochlores in oxidizing conditions, determined by faradaic efficiency, oxygen permeation and e.m.f. measurements at 973–1223 K, vary from 0.95 to 0.98, increasing when the temperature or oxygen partial pressure decreases. The oxygen pressure dependencies of the transference numbers and permeation fluxes can be adequately described by models derived from classical concepts for solid oxide electrolytes. The activation energies for the ionic and electron-hole transport in air are in the ranges 74–77 and 87–91 kJ/mol, respectively. Under a gradient of $10\%H_2 + 90\%N_2$/air, the average ion transference numbers of $(Gd,Ca)_2Ti_2O_{7-\delta}$ ceramics are not less than 0.97. The maximum power density obtained in a single model cell with a $Gd_{1.90}Ca_{0.10}Ti_2O_7$ electrolyte (thickness 1.0 mm), porous Pt electrodes, a $10\%H_2 + 90\%N_2$ mixture as a fuel, and air as an oxidant, was as low as 8–18 mW/cm^2 at 1123–1273 K. Linear voltage-current dependencies and impedance spectroscopic data indicate that such a low performance is due to a high ohmic contribution to the total potential drop in the fuel cells, resulting from the low conductivity of pyrochlore solid electrolytes.

Acknowledgements Financial support from the FCT, Portugal (PRAXIS and POCTI programs and the project BD/6827/2001), the INTAS (project 00276), and the Belarus State University is gratefully acknowledged.

References

1. Yamamoto O (2000) Electrochim Acta 45:2423
2. Chen TP, Wright JD, Krist K (1997) System analysis of oxide fuel cell unit. In: Stimming U, Singhal SC, Tagawa H, Lehnert W (eds) SOFC V. (Proceedings vol 97–40) The Electrochemical Society, Pennington, NJ, pp 69–78
3. Steele BCH (2001) J Mater Sci 36:1053
4. Tuller HL, Kramer SA, Spears MA, Pal UB (1996) US Patent 5509189
5. Holtappels P, Poulsen FW, Mogensen M (2000) Solid State Ionics 135:675
6. Tuller HL (2000) Materials design and optimization. In: Tuller HL, Schoonman J, Riess I (eds) Oxygen ion and mixed conductors and their technological applications. (NATO ASI series) Kluwer, Dordrecht, pp 245–270
7. Kramer SA, Tuller HL (1995) Solid State Ionics 82:15
8. Kramer S, Spears M, Tuller HL (1994) Solid State Ionics 72:59
9. Heider U, Jörissen L, Huggins RA, Witschel W (1996) Ionics 2:7
10. Kilner JA (2000) Solid State Ionics 129:13
11. Chen J, Lian J, Wang LM, Ewing RC, Boatner LA (2001) Appl Phys Lett 79:1989
12. Pirzada M, Grimes RW, Minervini L, Maguire JF, Sickafus KE (2001) Solid State Ionics 140:201
13. Wuensch BJ, Eberman KW, Heremans C, Ku EM, Onnerud P, Yeo EME, Haile SM, Stalik JK, Jorgensen JD (2000) Solid State Ionics 129:111
14. Williford PE, Weber WJ, Devanathan R, Gale JD (1999) J Electroceram 3:409
15. Kharton VV, Naumovich EN (1993) Russ J Electrochem 29:1297
16. Yaremchenko AA, Kharton VV, Naumovich EN, Tonoyan AA, Samokhval VV (1998) J Solid State Electrochem 2:308
17. Kharton VV, Figueiredo FM, Navarro L, Naumovich EN, Kovalevsky AV, Yaremchenko AA, Viskup AP, Carneiro A, Marques FMB, Frade JR (2001) J Mater Sci 36:1105
18. Kharton VV, Viskup AP, Yaremchenko AA, Baker RT, Gharbage B, Mather GC, Figueiredo FM, Naumovich EN, Marques FMB (2000) Solid State Ionics 132:119
19. Yaremchenko AA, Kharton VV, Naumovich EN, Marques FMB (2000) J Electroceram 4:235
20. Kharton VV, Yaremchenko AA, Viskup AP, Mather GC, Naumovich EN, Marques FMB (2000) Solid State Ionics 128:79
21. Kharton VV, Viskup AP, Figueiredo FM, Naumovich EN, Yaremchenko AA, Marques FMB (2001) Electrochim Acta 46:2879
22. Kharton VV, Marques FMB (2001) Solid State Ionics 140:381
23. Rodriguez-Carvajal J (1993) Physica B 192:55
24. Liu M, Hu H (1996) J Electrochem Soc 143:L109
25. Kharton VV, Tikhonovich VN, Shuangbao L, Naumovich EN, Kovalevsky AV, Viskup AP, Bashmakov IA, Yaremchenko AA (1998) J Electrochem Soc 145:1363
26. Kharton VV, Yaremchenko AA, Kovalevsky AV, Viskup AP, Naumovich EN, Kerko PF (1999) J Membr Sci 163:307
27. Kharton VV, Naumovich EN, Vecher AA (1999) J Solid State Electrochem 3:61
28. Kharton VV, Yaremchenko AA, Naumovich EN, Marques FMB (2000) J Solid State Electrochem 4:243
29. Steele BCH (2000) Solid State Ionics 129:95
30. Lee J-H, Mori T, Li J-G, Ikegami T, Komatsu M, Haneda H (2000) J Electrochem Soc 147:2822
31. Rickert H (1982) Electrochemistry of solids. An introduction. Springer, Berlin Heidelberg New York
32. Huang P, Petric A (1996) J Electrochem Soc 143:1644